Planta
https://doi.org/10.1007/s00425-019-03216-0

ORIGINAL ARTICLE

Raman spectroscopy as an early detection tool for rose rosette infection

Charles Farber[1] · Madalyn Shires[2] · Kevin Ong[2] · David Byrne[3] · Dmitry Kurouski[1,4]

Received: 30 May 2019 / Accepted: 15 June 2019

Abstract

Main conclusion **Hand-held Raman spectroscopy is a potential tool for a confirmatory, non-invasive, and non-destructive detection and identification of rose rosette disease. Using this spectroscopic approach, structural changes in roses that are associated with this viral infection can be revealed.**

Abstract The commercial rose shrub industry in the United States is one of the largest of its kind. All commercial rose varieties are susceptible to rose rosette disease (RRD), a deadly viral disease vectored by eriophyid mites. This disease is typically diagnosed visually and/or by PCR-based detection assays. The present work demonstrates that Raman spectroscopy can detect RRD in intact leaf tissue. It is shown that chemometric analysis can distinguish between spectra collected from symptomatic and asymptomatic tissue, as well as between healthy and asymptomatic tissue. This method will be useful as an initial screen for RRD prior to PCR analysis to help conserve reagents and save time.

Keywords Raman spectroscopy · Plant viruses · Rose rosette disease

Introduction

The garden shrub rose (*Rosa* spp.) industry in the United States is one of the largest of its kind, reporting over $200 Million in sales in 2014 (Census of Horticultural Specialties 2014, 2015). All commercial roses are susceptible to rose rosette disease (RRD), a deadly infection by *Rose rosette virus* (RRV) vectored by eriophyid mites (Laney et al. 2011; Pemberton et al. 2018; Byrne et al. 2018). As no treatment yet exists, rapid disease detection is necessary to prevent its propagation. Current diagnostics are based on initial visual inspection of the plant for symptoms and confirmation by various polymerase chain reaction (PCR)-based assays, including RT(real-time)-PCR and TaqMan RT-quantitative (q) PCR (Babu et al. 2018). These methods are time consuming, costly, and highly sensitive to contamination from environmental DNA and small quantities of organic solvents. PCR also requires initial design of primers based on known genetic sequences, which is not trivial for viruses. These limitations make alternative, yet highly sensitive, virus diagnostic methods desirable.

Raman spectroscopy (RS) is a non-invasive, non-destructive analytical technique that reveals the chemical structure of analyzed samples. For the most basic Raman experiments, little-to-no specific sample preparation and no reagents are required to acquire data. While frequently used in analytical chemistry, the method has seen application in fields from materials science (Cantarero 2015) to forensics (Virkler and Lednev 2009) and food science (Almeida et al. 2010). With the development of portable instrumentation, RS has seen expanded infield use (Kurouski and Van Duyne 2015).

Our group has recently demonstrated that RS could be used for detection of fungal pathogens on corn, wheat, and

Electronic supplementary material The online version of this article (https://doi.org/10.1007/s00425-019-03216-0) contains supplementary material, which is available to authorized users.

✉ Dmitry Kurouski
dkurouski@tamu.edu

[1] Department of Biochemistry and Biophysics, Texas A&M University, College Station, TX 77843, USA

[2] Department of Plant Pathology and Microbiology, Texas A&M University, College Station, TX 77843, USA

[3] Department of Horticultural Sciences, Texas A&M University, College Station, TX 77843, USA

[4] The Institute for Quantum Science and Engineering, Texas A&M University, College Station, TX 77843, USA

Published online: 20 June 2019

sorghum (Egging et al. 2018; Farber and Kurouski 2018). We showed that RS can not only distinguish and diagnose simple diseases, but also identify complex diseases caused by combinations of pathogens. We also provided additional evidence that Raman spectra are distinguishable between stages of a disease. In addition to fungal disease diagnostics, we have recently shown that RS can be used to detect insect larvae within beans, detecting not only their presence but also, using statistical models, their developmental stage (Sanchez et al. 2019a). Additionally, Yeturu and colleagues described the detection of *Abutilon mosaic virus* in the ornamental plant *Abutilon* sp. by associating variations in intensity to different stages of the infection (healthy and from early to late) (Yeturu et al. 2016). Together, these results suggest that RS may be favorable for confirmatory detection of RRD.

Materials and methods

Roses

Foliage from two varieties of ornamental roses was used in this study: The Double Knock Out® Rose and The Pink Double Knock Out® Rose (The Family 2019). The Double Knock Out® Rose is a shrub rose with a cherry-red bloom color. It is a continuous blooming plant and is self-cleaning. The plant maintains a boxy shape with its typical dimensions being 3–4 feet tall by 3–4 feet wide. The new growth on the plant is a red to purple color and the mature foliage is a purplish green color. ('Radtko', PP 16,202, CPBR 3104.) The Pink Double Knock Out® Rose is described similarly to the Double Knock Out® Rose, with noted differences being that the bloom color is pink, and the foliage is typically a mossy green, ('RadtkoPink', PP 18,507, CPBR 3757.).

Leaf samples were collected from plants located in five different locations in Oklahoma and Texas. Growing conditions were identical across all plants unless otherwise specified. Precautions were taken to avoid collecting leaves that show evidence of non-RRD-associated stress. All disease development stages were assigned based on visual inspection as described below:

Healthy samples (HL) were collected in College Station, TX from Double Knock Out plants, which were grown outdoors. Bed and plant upkeep were done at the discretion of landscape staff according to grower-recommended care guidelines. The absence of *Rose rosette virus* was confirmed by PCR testing (See below).

Asymptomatic, PCR positive samples (AS) were collected in College Station, TX from Pink Double Knock Out plants. The status of asymptomatic, PCR positive was assigned to the plant based on lack of observed symptoms and an RRV-positive PCR test.

Symptomatic samples were collected from Ferris, TX; Van Alstyne, TX; and Durant, OK from Double Knock Out and Pink Double Knock Out Plants. Symptomatic status was assigned based on visual observation and PCR. Symptomatic is defined as one or more rosettes on the plant and symptomatic stems.

PCR procedures

RNA extraction for RRV detection testing was conducted using a modified direct antigen protocol (Shires et al. 2018). Plant tissue was placed into an ELISA sample mesh bag and then homogenized in 1X phosphate-buffered saline with 0.05% Tween 20 (1X PBS-T-Agdia #00930). 1500 µL of homogenate was then transferred to a polypropylene PCR tube and incubated on ice for 2 min. Following incubation, the homogenate was removed, and the tube was washed five times with 1000 µL 1X PBS-T. The tube was then rinsed for the final time with 1000 µL 1X PBS-T to remove any remaining tissue residue, and then vigorously flicked/tapped to remove as much PBS-T residue as possible. The tube was then placed onto a 95 °C heat block for 1 min, and then immediately transferred back to the ice for 1 min. To elute the RNA, a master mix composed of 2 µL RNasin (Promega#N2511) and 30 µL water per tube was used. 32 µL of the mix was added to the tube, and then the tube was vortexed to facilitate elution of the RNA from the column surfaces. The tube was then centrifuged for 10 s and used for PCR testing.

RRV detection testing was performed using a One-Step RT-PCR kit (#210212, Qiagen, Valencia, CA). Amplification was carried out in 25 µL reaction mixtures containing ~ 20 ng of template RNA, 2.5 mM $MgCl_2$, 400 µM of each dNTP, 0.5 µM of each primer (see below) and performed in a Bio-Rad C-1000 Touch™ Thermal Cycler (Bio-Rad Laboratories, Inc., Hercules, CA) with the following program: lid temperature of 95 °C, incubation at 50 °C for 30 min for reverse transcription, incubation at 95 °C for 15 min to deactivate reverse transcriptase, 40 cycles of denaturing at 94 °C for 30 s, annealing at 51 °C for 30 s, extension at 72 °C for 60 s, and a final extension at 72 °C for 10 min.

The primary sequences (Di Bello et al. 2018) used to confirm the presence of the virus are as follows:

RRVF (5′-GCACATCCAACACTCTTGCAGC-3′)

RRVR (5′-CTTATTTGAAGCTGCTCCTTGATTTCC-3′)

Aliquots (5 µL) of PCR products were visualized by electrophoresis through 2% agarose gels for 1 h at 5 v/cm in 1X TAE buffer (40 mM Tris, 20 mM Acetate, 1 mM EDTA, pH 8.6). The sizes of the amplified DNA products were determined using 50–2000 bp DNA Markers

(HyperLadder™ 50 bp, Bioline, Memphis, TN). Expected product size is 271 bp. Presence/absence is determined based on bands, with faint bands being considered as inconclusive.

Raman spectroscopy

Raman spectra were acquired with an Agilent Resolve spectrometer equipped with an 830 nm laser. Each leaf was scanned 2–4 times (in halves for small leaves, quadrants for larger leaves) using 495 mW of power with a 1 s exposure and 1 accumulation. Approximately 30 leaves per class were measured, resulting in total of 808 spectra. Spectra were baselined automatically by the instrument software and imported into the MATLAB addon PLS_Toolbox 8.6.2 for statistical analyses. Averaged spectra for each group of plants along with their standard deviations are shown in the Figs. S1 and S2.

Results and discussion

Analysis of rose leaf spectra

The averaged rose leaf spectra (Fig. 1) exhibit vibrational bands that we assign to cellulose, xylan, lignin, carotenoids, and proteins, major structural components of plants. The bands at 520, 1049, and 1118 cm^{-1} can be assigned to glucose, which is a monomer of the cell wall component cellulose. The band at 1216 cm^{-1} likely originates from xylan, another polymeric sugar cell wall component. The spectra also have a band at 1610 cm^{-1}, which can be assigned to lignin. The bands at 1526 and 1000 cm^{-1} can be assigned to the C=C and CH_3 vibrations of carotenoids, respectively. The band at 1157 can be assigned to a combination of glycosidic linkage vibrations in starch and C–C vibrations in carotenoids. These results demonstrate that RS is sensitive to the highly abundant structural and pigment molecules in the leaves.

The 1650–1730 cm^{-1} spectral region primarily contains carbonyl stretching vibrations. In the healthy rose spectrum, we observed two bands in this region at 1669 and 1720 cm^{-1}. The 1669 cm^{-1} band, also known as the amide I band, is a general indicator protein in a sample. This suggests that RS may detect changes in the protein content of the leaves. The unambiguous assignment of 1720 cm^{-1} vibration is more complicated because many different carbonyl compounds, including esters, aldehydes, carboxylic acids, and ketones can have the carbonyl stretching vibration in this region depending on the chemical context of the carbonyl group. In a similar way, the exact molecules contributing to the bands in the 1287–1488 cm^{-1} region, which were assigned to CH, CH_2, and CH_3 vibrations, cannot be precisely identified, due to the ubiquity of these groups in biological molecules (Table 1).

Following normalization to the 1441 cm^{-1} band, which can be assigned to CH_2/CH_3 vibration, the spectra of each class were found to be largely identical in terms of intensities and frequencies of all vibrational bands. However, large

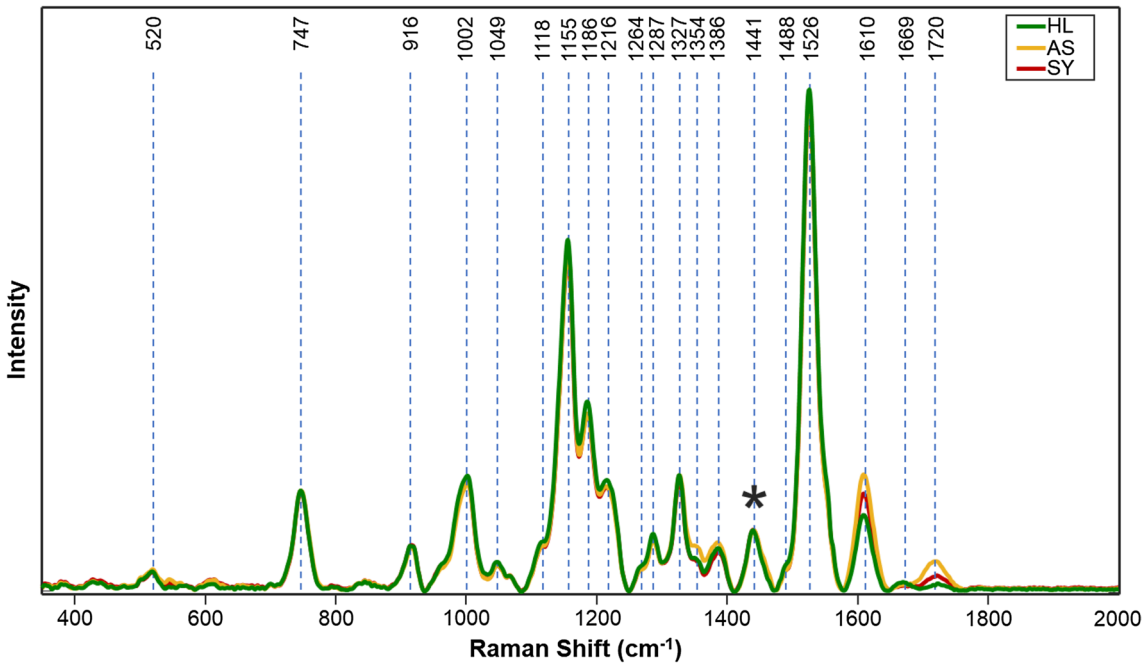

Fig. 1 Averaged spectra of all classes normalized to the 1441 cm^{-1} band (indicated with *). Inset: 1570–1770 cm^{-1} from normalized spectra

Table 1 Vibrational band assignments for rose leaf spectra

Band	Vibrational mode	Assignment
520	ν(C–O–C) glycosidic	Cellulose (Edwards et al. 1997)
740–747	γ(C–O–H) of COOH	Pectin (Synytsya et al. 2003)
905–918	ν(C–O–C) in plane, symmetric	Cellulose, lignin (Edwards et al. 1997)
1000	In-plane CH_3 rocking of polyene	Carotenoids (Schulz et al. 2005)
1048	ν(C–O) + ν(C–C) + δ(C–O–H)	Cellulose, lignin (Edwards et al. 1997)
1118	Sym ν(C–O–C), C–O–H bending	Cellulose (Edwards et al. 1997)
1157	C–C stretching; ν(C–O–C), ν(C–C) in glycosidic linkages, asymmetric ring breathing	Carotenoids (Schulz et al. 2005), carbohydrates (Wiercigroch et al. 2017)
1186	ν(C–O–H) next to aromatic ring + σ(CH)	Lignin (Agarwal 2014; Mary et al. 2012)
1216	δ(C–C–H)	Aliphatics (Yu et al. 2007), xylan (Agarwal 2014)
1264	Guaiacyl ring breathing, C–O stretching (aromatic)	Lignin (Cao et al. 2006)
1287	δ(C–C–H)	Aliphatics (Yu et al. 2007)
1327	δCH_2 bending	Aliphatics, cellulose, lignin (Edwards et al. 1997)
1354	$\delta(CH_2) + \delta(CH_3)$	Aliphatics (Yu et al. 2007)
1386	δCH_2 bending	Aliphatics (Yu et al. 2007)
1441	$\delta(CH_2) + \delta(CH_3)$	Aliphatics (Yu et al. 2007)
1488	$\delta(CH_2) + \delta(CH_3)$	Aliphatics (Yu et al. 2007)
1526	–C=C– (in-plane)	Carotenoids (Devitt et al. 2018; Adar 2017)
1610	ν(C–C) aromatic ring + σ(CH)	Lignin (Kang et al. 2016; Agarwal 2006)
1669	=O stretching, amide I	Proteins (β-sheet) (Devitt et al. 2018)
1720	C=O stretching	Esters, aldehydes, carboxylic acids, and ketones (Colthup et al. 1990)

intensity variations relative to 1441 cm^{-1} can be observed in the 1610 and 1720 cm^{-1} bands. In both cases, the healthy average shows the lowest intensity relative to the 1441 cm^{-1} band. The 1610 cm^{-1} band, previously assigned to lignin, might increase in response to infection (Liu et al. 2018). Alternatively, this band might be associated with the rapid growth phenotype (appearance of witches' brooms, excessive thorniness, enlarged canes) that is typical for RRD.

The 1720 cm^{-1} band is likely associated with plant stress response signaling molecules. Two major biotic stress hormones, jasmonic acid and salicyclic acid, are carboxylic acids, and thus could potentially be assigned to this band (Verma et al. 2016). The data presented here alone are insufficient to determine whether this is the case; further studies coupling mass and Raman spectrometries are required to confirm the identities of the carbonyl-containing molecules.

Our group has previously demonstrated that for some fungal pathogens, such as sorghum grain mold, the intensity progression of notable bands (cellulose, lignin, and carbohydrates) across disease stages had a clear trend (Egging et al. 2018). Based on this observation, it can be noted that the molecular interactions between plant hosts and pathogens vary depending on the nature of the infectious agent.

Based on rigorous visual inspection of the plants followed by PCR, it is reasonable to assume that each of the classes should be homogenous spectroscopically. However, following careful inspection of spectra, we found two distinct subgroups within the asymptomatic spectra (Figs. 2 and S3). One set of spectra (group I) exhibits higher intensity bands at the 1610 and 1720 cm^{-1}, which was previously observed

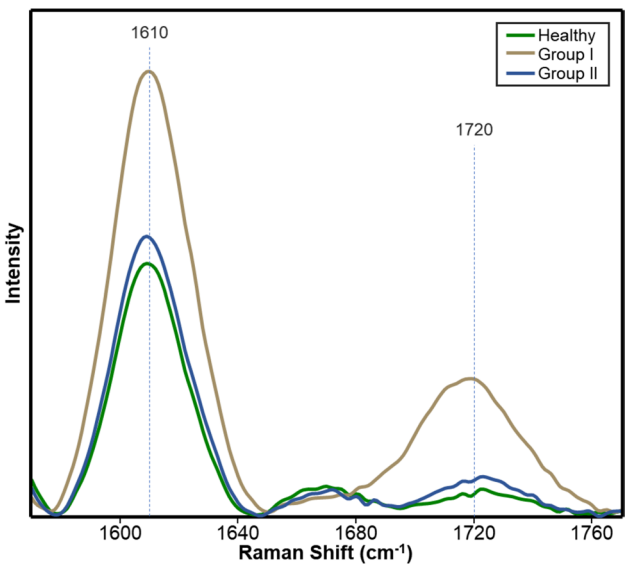

Fig. 2 Averaged spectra of the healthy and asymptomatic spectra. Asymptomatic is divided into two different categories based on the intensity of the 1720 cm^{-1} band. Normalized to the 1441 cm^{-1} band (see Fig. S3)

Table 2 Misclassification table for the SA model

	Members	Correct	Symptomatic	Asymptomatic
Symptomatic	103	89.3%	92	11
Asymptomatic	131	91.6%	11	120
Matthew's correlation coefficient	0.809			

in asymptomatic as one large group (Fig. 1). The other set of spectra shows lower intensity bands at these two bands, reminiscent of healthy spectra. Because our method is sensitive to concentration, the differences between these spectra could be explained by parts of the plant having different magnitudes of response to the virus. Additionally, RS may be sensitive enough to distinguish healthy from infected tissues within individual plants.

The question to ask is how specific and selective is this spectroscopic method for RRD. Our group has previously demonstrated the specificity of Raman on other experimental systems. We demonstrated that different pathogens of the same kingdom (in this case, fungi) are associated with distinct spectroscopic changes (Farber and Kurouski 2018). Additionally, we recently demonstrated that in the spectra of citrus tree leaves, responses to biotic and abiotic (nutrient deficiency) stresses are distinct from each other (Sanchez et al. 2019b). Although additional experimentation is needed to disentangle RRD from other biotic and abiotic stressors, we are confident that the observed spectral changes (Fig. 1) are specific for rose rosette because the RRD stage and absence of other stresses were confirmed by rose experts.

Statistical analysis

To determine whether the presence and degree of RRV infection could be determined from the Raman spectra, we conducted partial least squares-discriminant analysis (PLS-DA) (Eriksson et al. 2013). Using PLS_Toolbox 8.6.2., we built two PLS-DA models intended to be used in sequence: the first, SA (symptomatic–asymptomatic), distinguishes between symptomatic and asymptomatic spectra; the second, HA (healthy–asymptomatic), differentiates among the healthy and asymptomatic spectra (which were modeled as one class in SA). The SA model was built and validated using a total of 689 first derivative spectra (Figure S4), partitioned 66:34 into calibration and validation sets by the Kennard–Stone algorithm (Kennard and Stone 1969), resulting in a model with 7 latent variables (LVs). This model was used to generate a misclassification table (Table 2), which communicates the accuracy (defined as true positive rate) and the Matthew's correlation coefficient (MCC), a measure of a model's quality as a binary classifier (Chicco 2017). The first three LVs of the model explain 5, 86, and 0.9% of the variation between

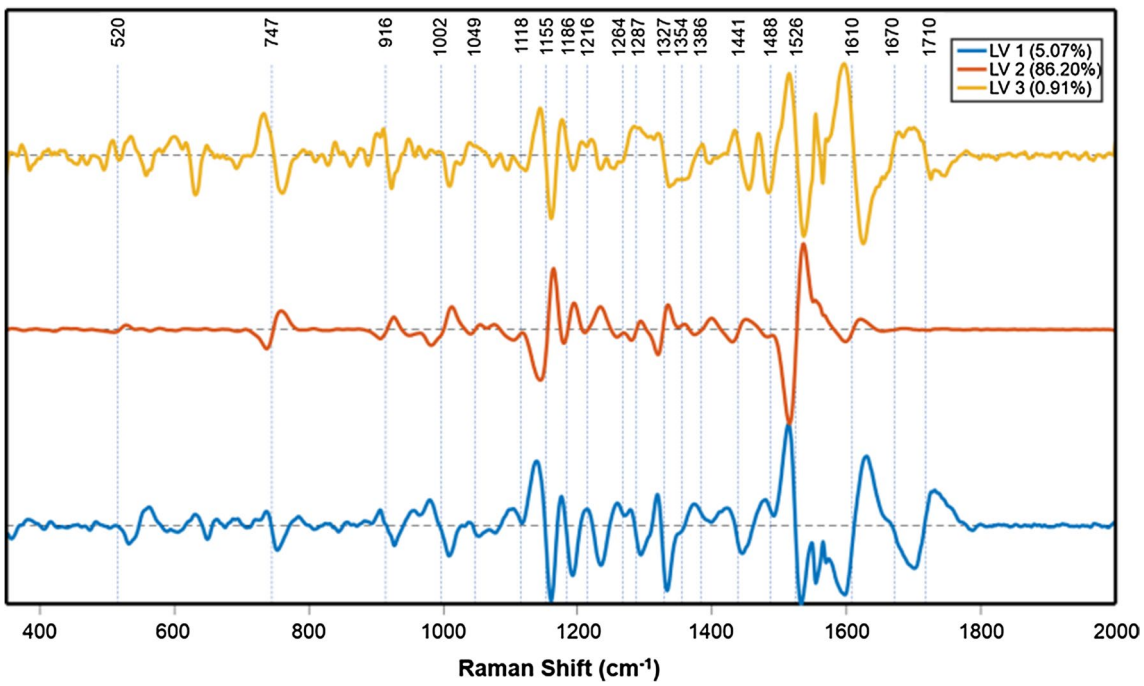

Fig. 3 Loadings plot of the first three LVs of the SA model, offset for clarity. Annotations indicate the centers of the peaks before the first derivative was taken. In the case of first derivative spectra, each standard Raman peak is defined by a minimum and maximum centered around a 0 point where the peak occurs in untreated Raman spectra

Table 3 Misclassification table for the HA model

	Members	Correct	Healthy	Asymptomatic
Healthy	59	98.3%	58	3
Asymptomatic	25	88%	1	22
Matthew's correlation coefficient	0.885			

the symptomatic and asymptomatic spectra, respectively. The loadings plot (Fig. 3) reveals the bands the model identified as important predictors of class. In this case, the plot of the second LV (which explains most of the class-to-class variation) is very similar to that of the typical rose spectrum suggesting that most of the classification was based on differences in intensity. From the first and third LVs, the previously discussed 1610 and 1720 cm^{-1} bands show greater importance. This corroborates our qualitative analysis of the spectra. From the misclassification table for SA (Table 3), we can see that, overall, the model performed well at this task. The MCC is close to one and the specific group accuracies are high. RS and chemometrics in combination can distinguish between symptomatic and asymptomatic plants.

The second model, which would accept spectra identified as asymptomatic by the first, differentiates between spectra from healthy and asymptomatic leaves, which could previously only be distinguished by PCR. For the purposes of this model, the group I and II spectra are treated as one group. This model was built using 248 mean-centered spectra, comprising the healthy and asymptomatic classes, and partitioned into calibration and validation sets as described for the previous model. The model, containing ten LVs, was used to generate a second misclassification table (Table 3) and loadings plot (Fig. 4). In this model, 39, 51, and 2.69% of the class-to-class variation is explained by the first three LVs. The loadings plots of the first two LVs are near mirror images of one another except for the 1610 and 1720 cm^{-1} bands, which continue to have moderate importance for the prediction. The third LV places greater importance on the aliphatic (1270–1400 cm^{-1}) bands, though relatively little of the variation is explained by this LV. These two models correctly assigned most spectra to their correct classes, indicating that a combination of RS and PLS-DA can detect the presence of RRD with high accuracy. This model also performed very well, with a large MCC and specific group accuracies. Despite the internal differences in the group of asymptomatic spectra, which were discussed above, our model could separate healthy and asymptomatic spectra.

Conclusion

The results demonstrated here show that RS, in the absence of other stress factors, can be used for the detection of RRV in rose leaves, and provides additional evidence that Raman can, in general, detect the presence of viruses in

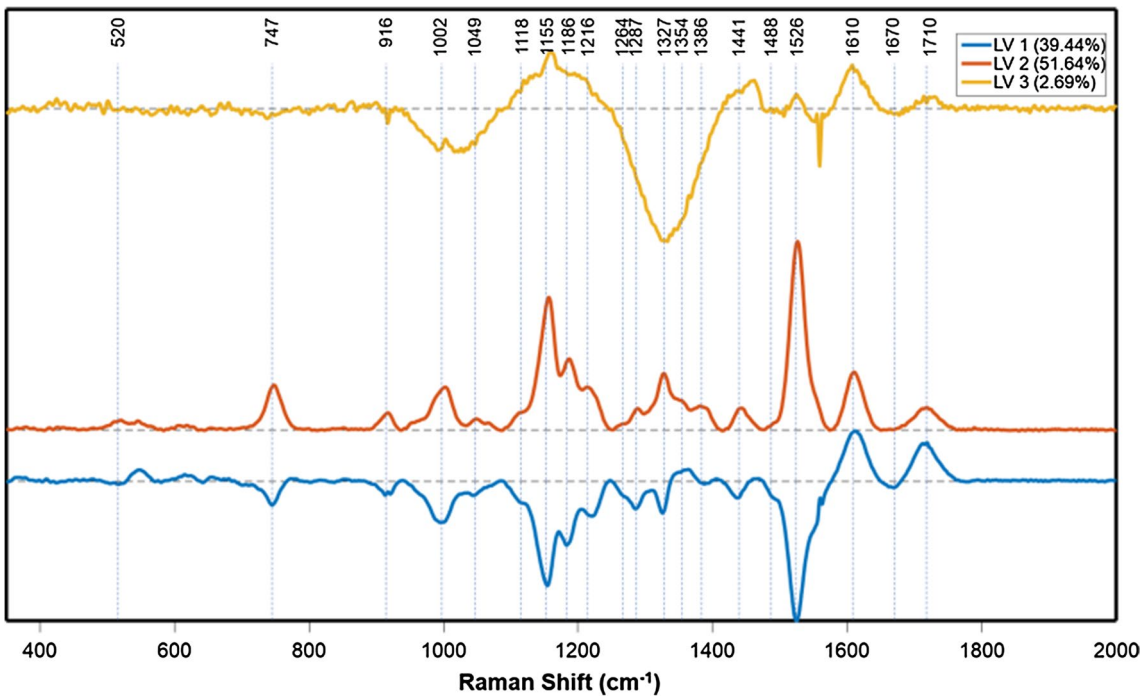

Fig. 4 Loadings plot for the HA model

a plant host. We also provide evidence that RS data can be used to track the development of diseases in plants as well as potentially determine the molecular changes associated with RRD. Additionally, using a combination of multivariate statistics and Raman, we found that the spectra of rose leaves with different degrees of infection could be differentiated with high accuracy. As these spectra were acquired with a portable instrument alone, this method could be applied to infield surveying as an initial screen before PCR, potentially saving time and valuable reagents.

Author contribution statement The authors acknowledge the contributions of Lee Sanchez, Mark Krimmer, Rohini Morey, and Zhongliang Xing for assistance in spectral acquisition, as well as Jake Ueckert for assistance in PCR testing and writing the rose plant methods.

Acknowledgements The authors are grateful for the financial support of Agrilife Research at Texas A&M and acknowledge the Governor's University Research Initiative (GURI) grant program of Texas A&M, GURI Grant Agreement No. 12-2016, M1700437.

References

Adar F (2017) Carotenoids—their resonance raman spectra and how they can be helpful in characterizing a number of biological systems. Spectroscopy 32(6):12–20

Agarwal UP (2006) Raman imaging to investigate ultrastructure and composition of plant cell walls: distribution of lignin and cellulose in black spruce wood (*Picea mariana*). Planta 224(5):1141–1153

Agarwal UP (2014) 1064 nm FT-Raman spectroscopy for investigations of plant cell walls and other biomass materials. Front Plant Sci 5:1–12

Almeida MR, Alves RS, Nascimbem LB, Stephani R, Poppi RJ, de Oliveira LF (2010) Determination of amylose content in starch using Raman spectroscopy and multivariate calibration analysis. Anal Bioanal Chem 397(7):2693–2701

Babu B, Knox G, Paret ML, Ochoa-Corona FM (2018) Rose rosette disease: recent advances on molecular diagnostic tools. HortScience 53(5):596–600

Byrne DH, Klein P, Yan M, Young E, Lau J, Ong K, Shires M, Olson J, Windham M, Evans T (2018) Challenges of breeding rose rosette–resistant roses. HortScience 53(5):604–608

Cantarero A (2015) Raman scattering applied to materials science. Procedia Mater Sci 9(Supplement C):113–122

Cao Y, Shen D, Lu Y, Huang J (2006) A Raman-scattering study on the net orientation of biomacromolecules in the outer epidermal walls of mature wheat stems (*Triticum aestivum*). Ann Bot 97:1091–1094

Census of Horticultural Specialties (2014) (2015) 2012 census of agriculture, vol 3. United States Department of Agriculture, Washington

Chicco D (2017) Ten quick tips for machine learning in computational biology. BioData Min 10(1):35

Colthup NB, Daly LH, Wiberley SE (1990) Introduction to infrared and Raman spectroscopy, 3rd edn. Academic Press, San Diego

Devitt G, Howard K, Mudher A, Mahajan S (2018) Raman spectroscopy: an emerging tool in neurodegenerative disease research and diagnosis. ACS Chem Neurosci 9(3):404–420

Di Bello P, Thekke-Veetil T, Druciarek T, Tzanetakis I (2018) Transmission attributes and resistance to rose rosette virus. Plant Pathol 67(2):499–504

Edwards HG, Farwell DW, Webster D (1997) FT Raman microscopy of untreated natural plant fibres. Spectrochim Acta A 53(13):2383–2392

Egging V, Nguyen J, Kurouski D (2018) Detection and identification of fungal infections in intact wheat and sorghum grain using a hand-held raman spectrometer. Anal Chem 90(14):8616–8621

Eriksson L, Byrne T, Johansson E, Trygg J, Vikstrom C (2013) Multi- and megavariate data analysis basic principles and applications, 3rd edn. Umetrics, Malmö

Farber C, Kurouski D (2018) Detection and identification of plant pathogens on maize kernels with a hand-held Raman spectrometer. Anal Chem 90(5):3009–3012

Kang L, Wang K, Li X, Zou B (2016) High pressure structural investigation of benzoic acid: Raman spectroscopy and X-ray diffraction. J Phys Chem C 120(27):14758–14766

Kennard RW, Stone LA (1969) Computer aided design of experiments. Technometrics 11(1):137–148

Kurouski D, Van Duyne RP (2015) In situ detection and identification of hair dyes using surface-enhanced Raman spectroscopy (SERS). Anal Chem 87(5):2901–2906

Laney AG, Keller KE, Martin RR, Tzanetakis IE (2011) A discovery 70 years in the making: characterization of the Rose rosette virus. J Gen Virol 92(7):1727–1732

Liu Q, Luo L, Zheng L (2018) Lignins: biosynthesis and biological functions in plants. Int J Mol Sci 19(2):335

Mary YS, Panicker CY, Varghese HT (2012) Vibrational spectroscopic investigations of 4-nitropyrocatechol. Orient J Chem 28(2):937–941

Pemberton HB, Ong K, Windham M, Olson J, Byrne DH (2018) What is rose rosette disease? HortScience 53(5):592–595

Sanchez L, Farber C, Lei J, Zhu-Salzman K, Kurouski D (2019a) Noninvasive and nondestructive detection of cowpea bruchid within cowpea seeds with a hand-held Raman spectrometer. Anal Chem 91:1733–1737

Sanchez L, Pant S, Xing Z, Mandadi K, Kurouski D (2019b) Rapid and noninvasive diagnostics of Huanglongbing and nutrient deficits on citrus trees with a handheld Raman spectrometer. Anal Bioanal Chem 411:3125–3133

Schulz H, Baranska M, Baranski R (2005) Potential of NIR-FT-Raman spectroscopy in natural carotenoid analysis. Biopolymers 77(4):212–221

Shires M, Ueckert J, Ong K (2018) Rose rosette virus: effective and low-cost extraction method. In: Paper presented at the ASHS Annual Conference, Washington, D.C

Synytsya A, Čopíková J, Matějka P, Machovič V (2003) Fourier transform Raman and infrared spectroscopy of pectins. Carbohydr Polym 54:97–106

The Family (2019) Star roses and plants. https://www.knockoutroses.com/family/ Accessed February 11 2019

Verma V, Ravindran P, Kumar PP (2016) Plant hormone-mediated regulation of stress responses. BMC Plant Biol 16:86–86

Virkler K, Lednev IK (2009) Raman spectroscopic signature of semen and its potential application to forensic body fluid identification. Forensic Sci Int 193(1–3):56–62

Wiercigroch E, Szafraniec E, Czamara K, Pacia MZ, Majzner K, Kochan K, Kaczor A, Baranska M, Malek K (2017) Raman and

infrared spectroscopy of carbohydrates: a review. Spectrochim Acta A 185:317–335

Yeturu S, Vargas Jentzsch P, Ciobotă V, Guerrero R, Garrido P, Ramos LA (2016) Handheld Raman spectroscopy for the early detection of plant diseases: abutilon mosaic virus infecting Abutilon sp. Anal Methods 8(17):3450–3457

Yu MM, Schulze HG, Jetter R, Blades MW, Turner RF (2007) Raman microspectroscopic analysis of triterpenoids found in plant cuticles. Appl Spectrosc 61(1):32–37